FEDSM2016-7866

CHARACTERIZATION OF THE CUSTOM-DESIGNED, HIGH REYNOLDS NUMBER WATER TUNNEL

Yasaman Farsiani
Oklahoma State University
Stillwater, Oklahoma, USA

Brian R. Elbing
Oklahoma State University
Stillwater, Oklahoma, USA

ABSTRACT

This paper reports on the characterization of the custom-designed high-Reynolds number recirculating water tunnel located at Oklahoma State University. The characterization includes the verification of the test section design, pump calibration and the velocity distribution within the test section. This includes an assessment of the boundary layer growth within the test section. The tunnel was designed to achieve a downstream distance based Reynolds number of 10 million, provide optical access for flow visualization and minimize inlet flow non-uniformity. The test section is 1 m long with 15.2 cm (6-inch) square cross section and acrylic walls to allow direct line of sight at the tunnel walls. The verification of the test section design was accomplished by comparing the flow quality at different location downstream of the flow inlet. The pump was calibrated with the freestream velocity with three pump frequencies and velocity profiles were measured at defined locations for three pump speeds. Boundary layer thicknesses were measured from velocity profile results and compared with analytical calculations. These measurements were also compared against the facility design calculations.

INTRODUCTION

Typical commercial recirculating water tunnels achieve a momentum thickness based Reynolds number (Re_θ) on the order of 10^3, which is not ideal for studying turbulent flow phenomena that could be Reynolds number dependent. On the other hand, the world's largest water tunnel, the U.S. Navy William B Morgan Large Cavitation Channel [1], can achieve a Re_θ on the order of 10^5, but the cost of operating is high. Thus the a relatively low-cost recirculating water tunnel that spans the gap between commercial water tunnels and the world's largest tunnel ($Re_\theta \sim 10^4$) was recently designed, built and installed at Oklahoma State University. The primary factors considered in the design of this tunnel were (1) to achieve a Reynolds number of 10 million per unit length, (2) optical access for flow visualization and (3) minimize inlet flow non-uniformity. The tunnel will primarily be used to study turbulent boundary layers with an emphasis on drag reduction applications. For example, current projects scheduled for the facility include the modification of a turbulent boundary layer with drag-reducing polymer solution, superhydrophobic drag reduction, helicopter wake control and bat ear aerodynamics. However, prior to performing these studies it is important that the facility without any model installed be characterized.

The characterization provided in the current work includes measuring the velocity uniformity within the test section, calibration of the test section centerline speed with the pump frequency and characterization of the boundary layer growth on the tunnel walls. These measurements will be compared with the calculations used to design the facility and the quality of the performance will be reported based on design specifications.

WATER TUNNEL OVERVIEW

Design Constraint and Specifications

The tunnel design has previously been discussed [2-3], but a brief overview of the design of the primary components is provided here for completeness. The specifications for a given water tunnel is driven by the target application for the facility and constraints imposed by various resource limitations. The current facility is located in the Experimental Flow Physics Laboratory at Oklahoma State University, which imposed various size limitations. As for any water tunnel, the primary components are (1) the test section, (2) the pump and (3) flow conditioning to minimize flow non-uniformity within the test section. In recirculating water tunnels, any unsteadiness can affect the flow quality, thus flow conditioning must be considered both upstream and downstream of the test section.

Test section design is typically driven by the desired application, operation range and instrumental suite (optical and mechanical access). The current test section has been designed to study flat plate turbulent boundary layers, which requires the cross-section to be sufficiently large that the developing boundary layer produces a negligible pressure gradient. The initial design was performed via a momentum integral analysis assuming a 1/7th velocity profile on a zero-pressure gradient flat plate [4], which was then iteratively solved accounting for the displacement thickness to estimate the pressure gradient. The final design is 1 meter long with a 15.2 cm (6-inch) × 15.2 cm (6-inch) square cross section. The test section walls are acrylic to allow optical access, and the stainless steel frame was designed such that direct line of sight was possible at the walls.

The nominal test section speed range is from 1 to 10 m/s, which cavitation is a likely issue at the higher end of this range. For example, using the above momentum integral analysis to estimate the pressure distribution at 10 m/s results in a cavitation number (Ca) of 1.4 at the test section mid-point ($x = 0.5$ m). The smaller the number the more sensitive the flow-field will be to cavitation around any edge (e.g. bolt holes). Consequently, the tunnel is designed to be pressurized up to 276 kPa (40 psi) above atmospheric pressure. This increases Ca to 3.8 at the maximum test speed. The system is also plumbed with a vacuum pump to achieve pressures below atmospheric, which can be useful for degassing the water as well as studying caviation. However, the pressure vessel volume should be increased from the current configuration if tunnel operation below atmospheric pressure is desired.

Important parameters in the design of nozzle sections include the contraction ratio, length and shape, which must be carefully selected to get the best flow uniformity and a low turbulence level. The primary flow conditioning features are a series of honeycombs, settling chambers and a contraction. The honeycomb sizes were selected based on experimental results provided in Lumley & McMahon [5]. The upstream and downstream honeycomb is 19 mm (cell size) × 610 mm (length) and 6.4 mm (cell size) × 152 mm (length), respectively. The reason for adding the second stage was because the inlet turbulence level is unknown *a priori* and the initial stage sizing can be used to estimate the length scale of the largest turbulent structures. While the honeycomb breaks up turbulent structures, it also generates a turbulent wake downstream, which is why it is recommended that a settling chamber be located downstream to utilize viscous decay to suppress the turbulent flow [6-7]. Since a minimum length of 30-40 cell diameters is required, the upstream and downstream settling chambers are 594 mm (31 diameters) and 254 mm (40 cell diameters), respectively. Following the second honeycomb's settling chamber is a 740 mm long 8.5:1 area contraction, which reduces the turbulence intensity and increases the flow speed [8]. The contraction profile shape is a 5th order polynomial curve [9].

The water tunnel cross-sectional area is at a minimum in the test section, thus the flow must pass through a diffuser (or a series of diffusers) following the test section to return to the contraction inlet area. It is desirable to increase the area as soon as possible to minimize losses. However, the diffuser half-angles must be kept under 4° to prevent flow separation [10]. Consequently, three diffuser sections were used to complete the loop. The first is placed immediately downstream of the test section and the remaining two are located upstream and downstream of the pump section.

The pump generates the required pressure differential to overcome the system losses at the desired volumetric flow rate. Thus the pump and motor size selection is dependent on the entire loop design, which required an iterative design process. Figure 1 and Table 1 provides the final loop design along with the corresponding components. The entire tunnel was fabricated from stainless steel except for the fiberglass contraction and diffuser downstream of the test section. The final loop design required a pressure differential of 300 kPa (100 ft H_2O) to produce 0.28 m^3/s (4500 GPM), which is achieved with a 112 kW (150 hp) centrifugal pump (S10B12A-4, Patterson). The speed can be varied with a variable frequency drive. Additional facility and component design details are in Daniel [2].
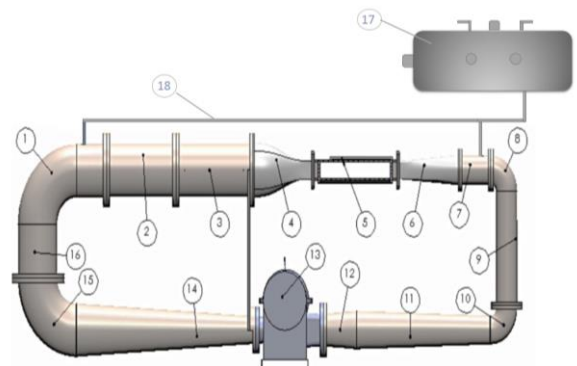
Figure 1. Schematic of the recirculating water tunnel. Numbers correspond to items listed in Table 1.

Table 1. List of individual water tunnel components.

No.	Description	No.	Description
1	Elbow 1	10	Elbow 3
2	Honeycomb	11	10″×12″ Rolled Cone
3	Settling Chamber and Honeycomb	12	Pump Inlet Pumping
4	Contraction	13	Pump and Motor
5	Test section	14	10″×20″ Rolled Cone
6	Diffuser	13	Elbow 4
7	Straight Pipe	16	Up Leg
8	Elbow 2	17	Pressure vessel
9	Down leg piping	18	Air extraction plumbing

Installation

The installation process included considerations related to the structural integrity (facility and building), assembling

procedure of the tunnel components and addition of structure for personnel and equipment access. The Experimental Flow Physics Laboratory is located in the Advanced Technology Research Center (ATRC) on the campus of Oklahoma State University. The ATRC building considerations for the tunnel installation included certifying the floor loading capacity, providing electrical access and plumbing for the water supply. The structural integrity of the ATRC floor was a concern because the estimated weight of the filled tunnel is 5,510 kg (12,150 lb), which requires that load to be properly distributed to prevent damage to the building. Since the tunnel is installed in a vertical orientation, the weight is carried using 3 support frames constructed from I-beams as shown in Figures 3 and 4. These three frames have 6 contact locations, 3 on the top leg and 3 on the bottom leg. Due to the large size and weight of these components and the precision required to complete the loop, it was critical to have a well-defined plan for assembling the complete loop. First, a concrete slab was laid to carry the weight of the tunnel. The pump and motor were then fixed in place on the foundation as well as the support structures. The lower leg of tunnel was connected with the pump and positioned on the structural supports with a hoist. A pair of ¼-ton push trolleys (CBTP-0025) with manual hoists were used to assemble the side legs and flow conditioning units on the top leg of the tunnel. The same hoists were used to lift the contraction-test section-diffuser assembly into place between the side legs to complete the loop. Throughout this installation process it was critical to provide additional support structures to ensure safety as well to regularly confirm that each component is properly leveled. Test section acrylic walls were the final pieces installed.

A 3-inch NPT port upstream of the pump inlet was plumbed to a three-way-valve that allows filling from the ATRC cold water line or draining. The water line has had particle filters installed to minimize the size of particles in the water. There is an additional drain pipe located on the 90° elbow on the lower leg downstream of the pump, which is used to drain the remaining water in the lower part of the tunnel.

The two primary objectives with the electrical installation was supplying the pump motor with sufficient power and isolating the variable frequency drive from the rest of the building. The 150 hp pump motor is powered from the building's 495 V line. However, the variable-frequency drive (VFD) used to control the motor frequency is rated for 460 V. Discussion with the manufacturer confirmed that the VFD (EQ7-4150C, Teco) could be operated up to 480 V. Fortunately, the an isolation transformer (423-D600-048, Jefferson Electric) was installed between the ATRC 495 V line and the VFD controller to prevent frequencies other than 60 Hz from being put onto the ATRC electrical system. The isolation transformer is also able to reduce the voltage to 480 V.

Pressure Control System

As previously mentioned, the pressure in the tunnel needed to be varied for the cavitation concern at higher test speeds. The pressure regulation system included a pressure vessel (AR8020, Campbell Hausfel) mounted on the ceiling of the laboratory. It has a total capacity of 0.098 m³ (26 gal). The vessel has a maximum operating pressure of 1,200 kPa (175 psi) and several ports of various sizes. A schematic of the pressure vessel is provided in Figure 2 along with the various connections. The pressure vessel is plumbed to the tunnel via a ¾-inch NPT pipe opening on the bottom of the vessel, which allows the vessel to be partially filled with water when filling the tunnel. There are two drain lines plumbed to the vessel, one at the bottom of the tank and the other at the vessel centerline. When filling the tunnel, the centerline drain will be opened while the bottom drain will be closed. This provides a path for the air in the tunnel to vent out of the loop while the tunnel is being filled.

Using the pressure vessel when filling or draining the tunnel, the second line is open to atmospheric pressure to allow for pressure recovery. The final line is connected to a vacuum pump to decrease the water pressure within the pressure vessel and the tunnel. This is the method to degas water for cavitation concerns. The plumbing is also arranged so that the tank can be filled with water independent of the water tunnel and degassed water can be collected for other experiments. The pressure can be monitored with a pressure gauge at the vacuum pump.

While running the tunnel at atmospheric pressure, air extraction from the flow loop was accomplished using the ports downstream and upstream of the test section at the highest points. By opening the pipe valve, the remaining air is removed from the tunnel.
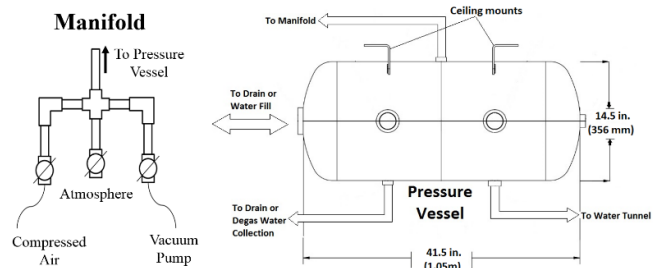
Figure 2 Schematic of the pressure manifold and Schematic of the pressure vessel along with the various connections [3].

Figure 3. Completed water tunnel installed at Oklahoma State University in the Experimental Flow Physics Lab.

Platform

After installing and assembling the complete tunnel. There was a need for a platform for personnel as well as positioning of the instrumentation that will be used for experiments. Experimental tools that are currently used for this tunnel were considered. The two primary instrumentations are (1) a polymer delivery system for drag reduction studies and (2) a PIV system for flow visualizations and velocity measurements. The test section is more than 2 meters above the ground, which requires that on each side a 0.76 m (30-inch) tall platform be constructed to allow individuals to comfortable work on the test section. In addition, a 61 cm (width) × 122 cm (length) × 5.8 cm (height) optics table (B2448FE, ThorLabs) was installed approximately 0.3 m below the test section for mounting components of the PIV system (e.g. lasers, cameras and sheet optics). The installed platform and optics table is shown in Figure 3.
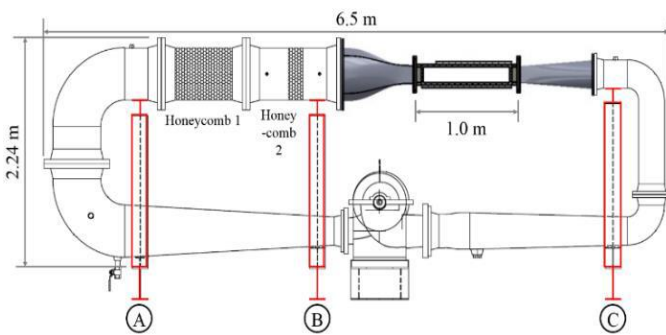
Figure 4. Schematic of the water tunnel with support structures.

Control and Circuit Ancillaries

For further experiments in the tunnel there is a need for controlling the test section status during the experiments. The control system makes extensive use of modern computer and electromechanical control, with automation of measurements implemented on the defined locations within test section. The

parameters such as the pump frequency, dimensional velocity and pressure, and the test section cavitation number and Reynolds number can be changed in order to control the test section velocity and pressure in a range of modes. These parameters can be all controlled during experiments by design and manufacturing a control table.

FACILITIES AND EXPERIMENTAL METHOD

As previously stated, this new custom designed recirculating water tunnel needs to be characterized before using it for testing any model. At the end of each day of testing the water was completely drained from the test section and refilled with fresh water prior to testing the next day. The air was scavenged from the tunnel prior to data collection. Measurements were acquired within the test section at a mean spanwise location and various stream-wise locations to analyze the flow quality, velocity profiles and boundary layer growth. Measurements were conducted with a state-of-the-art particle image velocimetry (PIV) system. The PIV system includes multiple lasers including a Nd:YLF single cavity diode pumped solid state laser (DM30-527, Photonics Industries) and a 532 nm Nd:YAG laser (Gemini 200, New Wave Research). It also has an assortment of cameras including two high resolution sCMOS cameras (Imager sCMOS, LaVision) and two high-speed CMOS cameras (M110, Phantom). The acquisition and processing is performed with a commercial software package (DaVis 8, LaVision).

For current experiment, the PIV system used the 532 nm Nd:YAG laser and a CCD camera. The laser beam was converted into a sheet using a cylindrical lens. The laser sheet illuminated 18 μm tracer particles added to the water tunnel (im30K hollow glass spheres, 3M). The scattered light from the particles was then captured with the CCD camera, which took two images of the flow-field. The high-speed CMOS camera has a 1280×800 pixel resolution, 20×20 μm pixels, 12-bits digital output, 60 GB of onboard storage and can acquire images at 1630 frames/sec at full resolution. The cross-correlation between the two images was locally performed using commercial software (DaVis 8.2, LaVision) to determine the two dimensional velocity vector fields. The current PIV setup is schematically shown in Figure 5. For each condition 100 image-pairs were taken and averaged to produce the average vector field.

The laser and optics were set up outside the walls of the test section. For characterization tests the laser was shooting from the bottom and the camera captured the front wall view.
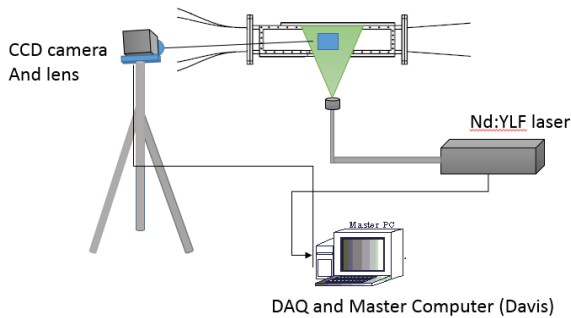
Figure 5. Schematic of PIV system used to measure the velocity distribution within the test section.

During testing a difference in the measured velocity was noticed in between runs for different laser power levels. The interframing time between the two laser pulses was identified as the main contributor to this deviation. For the processing of the images much care was taken to realize enough particles within a single interrogation window to enable clear correlations. Several different interrogation window sizes were evaluated based on defined validation criteria.

TUNNEL CHARACTERIZATION

Test section flow quality

The first necessary analysis is to evaluate the flow quality within the test section. This section presents the experimental velocity vector fields from the PIV system. The coordinate used throughout testing has the X axis aligned with the streamwise direction, Y axis aligned in the vertical direction and the Z axis in the horizontal transverse direction completing the right-handed coordinate system. The origin is located at the center of the test section inlet. The velocity measurements were acquired at 9 different planes within the test section. Each with a nominal field-of-view (FOV) of 0.1 m × 0.12 m. The test matrix for characterization process is provided in Table 1. Each location represents the center of the measurement plane. The plane locations are illustrated in Figure 6 by "P#".

Table 2. Matrix of conditions tested during the water tunnel characterization.

location	X (m)	Y (mm)	Pump speed (Hz)	FOV (m²)
1	0.15	71	5	0.1×0.12
2	0.5	0	7	0.1×0.12
3	0.9	-0.71	10	0.1×0.12
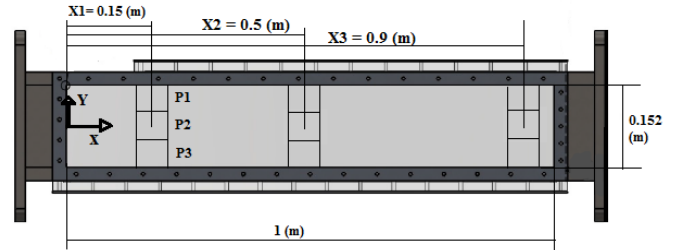
Figure 6. Test section schematic illustrating measurement locations.

Figure 7 shows an example of an interrogation window within a raw PIV image. A number of particles, nearly equally distributed, are visible with white dots. After image pre-processing to minimize image noise, multi-grid processing was performed. The multi-grid approach started the correlation process at an interrogation window size of 128×128 pixels that was then iteratively reduced to a final window size of 24×24 or 16×16 pixels with 50% overlap. The final window size provided acceptable results.
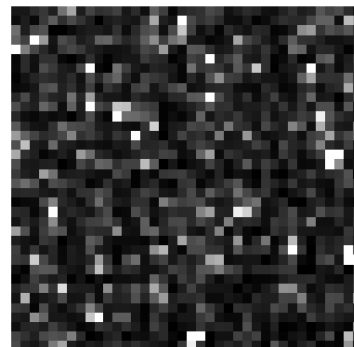
Figure 7. Raw PIV image zoomed into 32×32 pixels to show seeding density.

One measure of the quality of a water tunnel is the velocity uniformity. The total number of wall-normal vectors at each X location was 672 with nominally 650 of them being outside the boundary layer. Quality of the flow could be shown with flatness of velocity profiles for the flow outside of the wall boundary layers. Figure 8 shows velocity profiles at two X locations (near inlet and outlet) spanning the entire height of the test section. The overlay of the velocity profiles derived from the planes (P1, P2 and P3) at the same location show the flatness of the velocity profiles outside the wall region. In addition, this illustrates the accuracy of the current measurement technique. The resulting averages and standard deviations of these freestream velocity profiles are reported in Table 3. As seen in Figure 8, velocity fluctuations increase at higher pump frequencies and downstream locations as expected. The flatness of the velocity profiles is desirable.

Table 3. Mean and standard deviation of the velocity profiles outside of wall region in m/s.

f (Hz)	X1		X2		X3	
	Avg	Std	Avg	Std	Avg	Std
5	1.65	0.003	1.68	0.0035	1.70	0.005
7	2.31	0.004	2.35	0.0055	2.36	0.015
10	3.31	0.012	3.39	0.0055	3.42	0.019
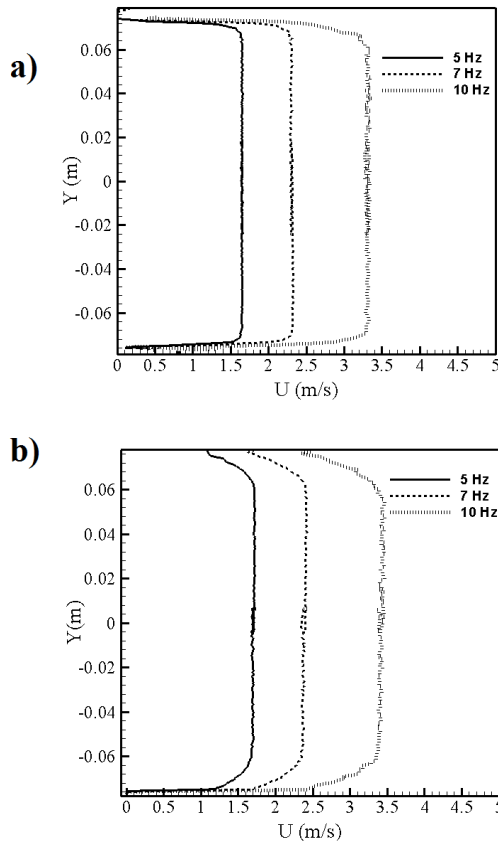
Figure 8. Velocity profiles for different pump frequencies at a) X1 and b) X3 spanning the entire test section height (Y).

In Figure 9 the standard deviations of the mean velocities from outside of the wall region are scaled with the mean velocities for the fixed X locations. The X locations are also scaled with average of boundary layer thicknesses for each speed. This shows both the increasing fluctuations with increasing speed as well as downstream distance. Over all conditions tested the velocity fluctuations fall between 0.2% and 0.5%. These levels are approaching the uncertainty of the measurement method, which suggests a more precise measurement (i.e. hot-wire anemometry) is needed to precisely quantify the turbulence levels.
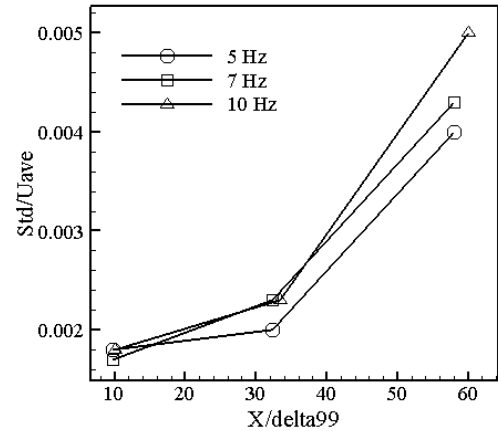
Figure 9. Scaled standard deviation of the averaged velocity profiles outside of the wall region.

Boundary Layers

The boundary layer growth on the test section walls was measured at each downstream measurement location. The boundary layer thickness was determined from the averaged velocity fields. Table 4 provides a list of the boundary layer results. These results are important for the design of future experiments.

Table 4. Boundary layer thickness values at different locations and speeds.

Location	Motor Frequency (Hz)	δ (mm)	
		P1	P3
X1	5	11	10
	7	10.6	9.32
	10	11.5	10.9
X2	5	16	15
	7	16	14.9
	10	16	14
X3	5	23	20
	7	18	18
	10	15.30	17.5

Velocity profiles at two stream-wise locations were extracted from the velocity vector fields. It should be mentioned that the velocities near the wall were difficult to measure using PIV. All of these profiles should have begun at a velocity of zero, but here the profiles did not show this because of inaccurate measurements near the wall. Figure 10 and 11 shows the velocity profiles at different locations of the test section. In each of the figures, velocity profiles for 3 different pump frequencies are compared. For the same X locations, the velocity profile at the top and bottom walls are relatively similar. Increasing pump frequency and distance from the inlet affects the boundary layer thicknesses reported in Table 4. As

expected, boundary layer thickness increases with increasing downstream distance.

a)

b)
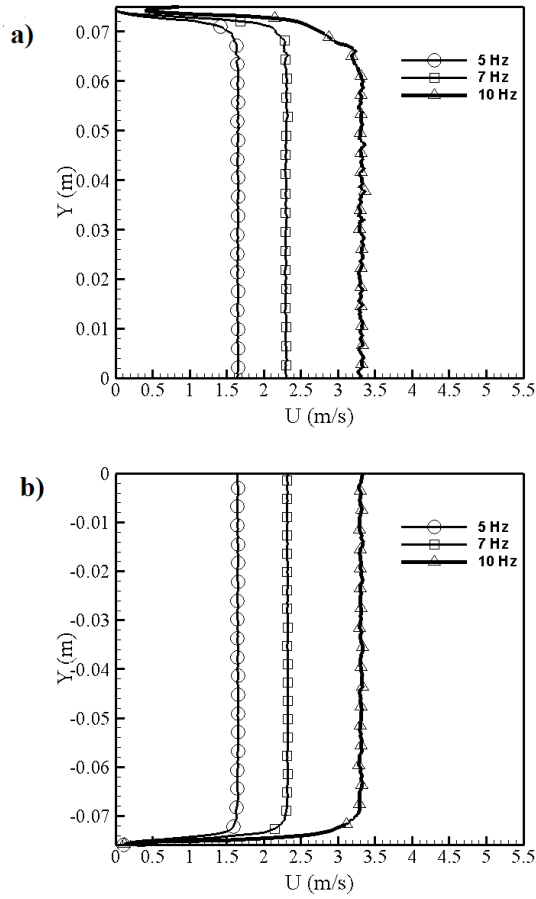
Figure 10. Velocity profiles acquired at X1 over the range of speeds tested at (a) P1 and (b) P3. For clarity only 1 of every 10 vectors has a marker.

a)

b)
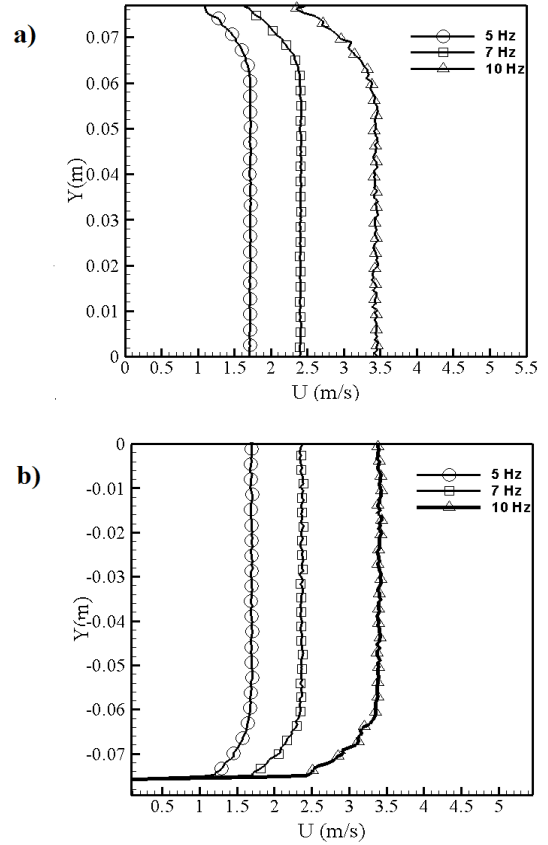
Figure 11. Velocity profiles acquired at X3 over the range of speeds tested at (a) P1 and (b) P3. For clarity only 1 of every 10 vectors has a marker.

The velocity profiles for P1 and P3 at X2 are scaled with the 99% boundary layer thickness (delta) and the freestream speed (U) in Figure 12. This scaling requires that the normalized velocity profile at one boundary layer thickness would be 0.99 of the freestream velocity. The plot (a) and (b) shows the normalized velocity profiles for three frequencies. As expected, the boundary layer thickness decreases with increasing pump speed and also the fluctuations of the velocity are higher at higher speeds.
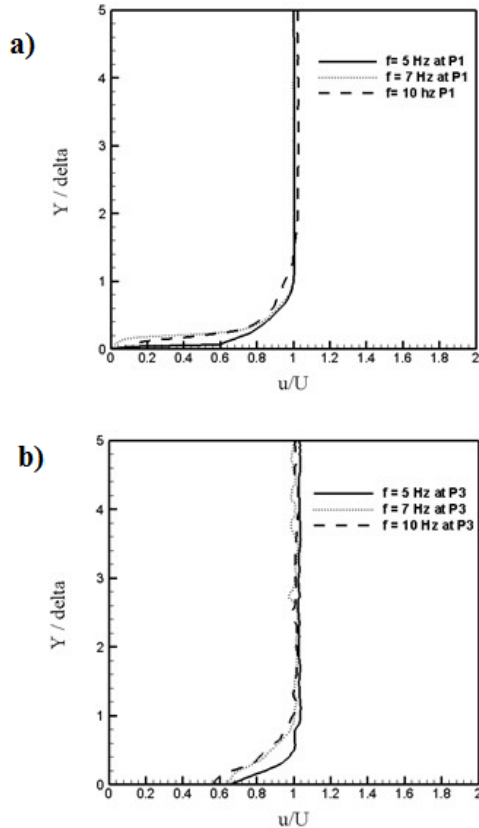
Figure 12. Normalized velocity profiles acquired at X2 over the range of speeds tested at a) P1 and b) P3.

Pump Calibration

To characterize and calibrate the variable frequency pump, averaged velocity components were measured and plotted versus pump frequency for the defined locations. Figure 13 shows the pump frequency versus averaged x-velocity in the P2 measurement plane, which is outside of the wall region. The averaged velocities at each *X* location gives the freestream velocities shown in Figure 13. Deviations of X-velocity is very low at all locations, especially at the inlet. The standard deviation is shown with the errorbars, which shows that with increasing downstream distance the fluctuations of the velocity increases. At all locations, freestream velocity versus pump speed are in a good agreement and the resulting calibration equation from these data is

$$U = 0.3437f - 0.0442 \qquad (1)$$

Figure 14 illustrates the averaged X-velocities at different locations for the three pump frequencies tested. This shows that the average centerline velocity gradually increases with increasing downstream distance. This growth also increase with increasing tunnel speed (i.e. motor frequency).
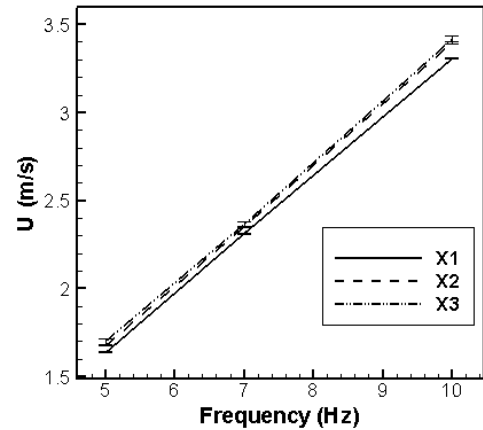
Figure 13. Centerline free-stream velocity at positions 1, 2 and 3 plotted versus the pump motor frequency. This establishes the calibration between the motor input and the test section speed.
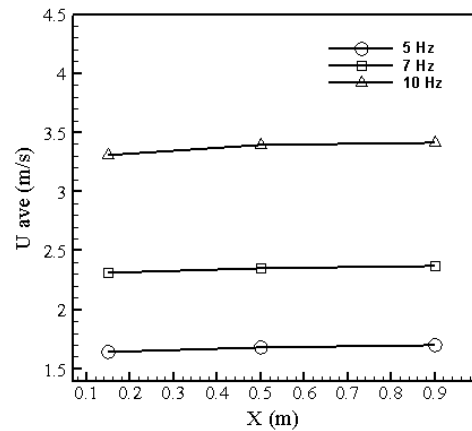
Figure 14. Averaged X-velocity at different X-locations for the 3 pump speeds tested.

PUMP DESIGN VALIDATION

The test section sizing resulted in a pump capacity requirement of 4500 GPM. Pressure head loss estimates (30 ft of head.) for all the components in the water tunnel flow loop provided the required pressure difference at the given flow rate. The final motor selection was upsized to 150 hp, which produced a pressure head of 100 ft to accommodate unaccounted losses due to non-uniformity and swirl in the flow. The performance curve for this pump is shown in Figure 15 is consistent with the motor power calculations that were based on the pressure loss estimates. The pump was designed such that at a frequency of 30 Hz the test section speed would be 10 m/s. To validate the design, Equation (2) was used to estimate the freestream speed at the design condition. Based on this calibration, at a pump angular speed of 30 Hz, the velocity would be 10.2 m/s. Thus current estimates show only a 2%

8

deviation between the target design condition and the expected maximum tunnel speed. This is exceptionally good agreement given that a factor of 3.2 was applied to the calculated losses within the tunnel. This was done during the design phase because historically calculations of the individual major and minor loses under-predicts the actual system loses.
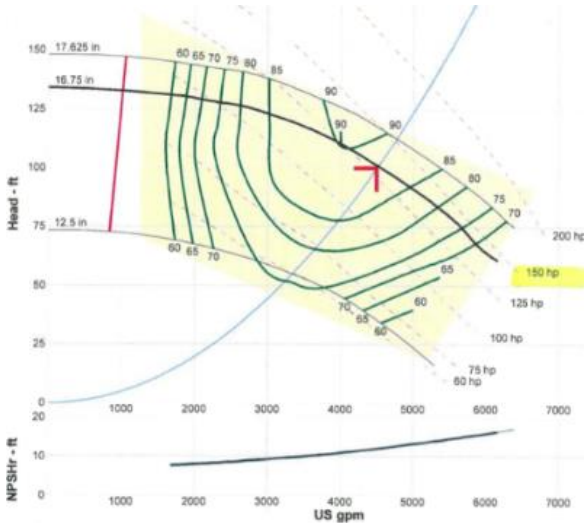
Figure 15. Pump Curve for the Centrifugal Pump.

CONCLUSION

Characterization of the custom designed water tunnel was performed, which is required for planning future experiments in the facility. The characterization included the verification of the test section design (flow uniformity), velocity distribution within the test section and pump calibration. Several conclusions can be drawn from this work:

(1) A calibration curve between the centerline test section velocity and the pump motor angular speed was produced and provided in Equation (1). While there was a deviation between this relationship and that obtained from the test section inlet, Equation (1), the deviation is not significant and either relationship can be used as a nominal test section speed.

(2) Due to pressure control limitations, the tunnel has not been taken to the maximum speed to confirm the tunnel design. However, use of the calibration curve, Equation (1), can be used to estimate the test section speed at the design condition of 30 Hz assuming the relationship remains linear. The deviation between the calibration curve and the design condition is 2%, which is in excellent agreement.

(3) The boundary layer forming on the top and bottom of the test section is nearly symmetric. This was determined from velocity profiles and boundary layer thickness at different locations measured on the top and bottom tunnel walls. Overlaying the velocity profiles from top and bottom sections at same locations along the test section and small standard deviation from the averaged velocity of velocity

gradient outside of the wall region proves the flatness of velocity profiles and flow uniformity.

The current manuscript only reports the mean profiles. However, it is important to report the uncertainty in the velocity measurements and turbulence intensity [11]. Efforts will allow the turbulence intensity within the test section also to be reported**.**

REFERENCES

[1] Park, JT, Cutbirth, J, Brewer, WH (2005) "Experimental methods for hydrodynamic characterization of a very large water tunnel," *ASME Journal of Fluids Engineering*, **127**(6), 1210-1214 (doi:10.1115/1.2060740).

[2] Daniel, L (2014) "Design and installation of a high Reynolds number recirculating water tunnel," M.S. Thesis, Oklahoma State University, USA.

[3] Daniel, L, Mohagheghian, S, Dunlap, D, Ruhlman, E & Elbing, BR (2015) "Design of a high Reynolds number recirculating water tunnel," *Proceedings of the ASME 2015 International Mechanical Engineering Congress and Exposition*, IMECE2015-52030, Houston, TX (Nov 13-19).

[4] White, FM (2006) *Viscous Fluid Flow*, 3rd Ed., McGraw Hill, Inc., 430-438.

[5] Lumley, JL & McMahon, JF (1967) "Reducing water tunnel turbulence by means of a honeycomb," *ASME Journal of Basic Engineering,* **89**, 764-770.

[6] Loehrke, RJ & Nagib, HM (1976) "Control of free-stream turbulence by means of honeycombs: A balance between suppression and generation," *ASME Journal of Fluids Engineering*, **98**(3), 342-355.

[7] Nagib, HM, Marion, A & Tan-atichat, J (1984) "On the design of contractions and settling chambers for optimal turbulence manipulation in wind tunnels," *Proceedings of the 22nd Aerospace Sciences Meeting*, AIAA Paper 84-0536 (doi: 10.2514/6.1984-536).

[8] Barlow, JB, Rae, WH Jr. & Pope, A (1999) *Low-Speed Wind Tunnel Testing*, 3rd Ed., John Wiley & Sons, New York.

[9] Bell, JH & Mehta, RD (1988) "Contraction design for small low-speed wind tunnels," *NASA STI/Recon Technical Report*, N89-13753.

[10] Nedyalkov, I (2012) "Design of contraction, test section and diffuser for a high-speed water tunnel," M.S. Thesis, Chalmers University of Technology, Sweden.

[11] ITTC (2014) "Guideline on the uncertainty analysis for particle imaging velocimetry," *International Towing Tank Conference (ITTC) Recommended Procedures and Guidelines*, 7.5-01- 03-03.